Unnexin is a protein subunit of a large-pore channel expressed by unicellular organisms

Juan Güiza[a], Francisco Solís[b], Bernardita Valenzuela[b], Duxan Arancibia[b], Pedro Zamorano[b], Jorge González[c], Jonathan Saavedra[d], Alan Neely[d] (ID),
Magdiel Salgado[d], Agustín D. Martínez[d], Juan C. Sáez[d,1], and José L. Vega[a,e,1]

Cells of vertebrate and invertebrate organisms express proteins specialized in membrane channel–based cell–cell communication that are absent in unicellular organisms. We recently described the prediction of some members of the large-pore channel family in kinetoplastids, consisting of proteins called unnexins, which share several structural features with innexin and pannexin proteins. Here, we demonstrated that the unnexin1 protein (Unx1) is delivered to the cell membrane, displaying a topology consisting of four transmembrane domains with C and N termini on the cytoplasmic side and form large-pore channels that are permeable to small molecules. Low extracellular Ca^{2+}/Mg^{2+} levels or extracellular alkalinization, but not mechanical stretching, increases channel activity. The Unx1 channel mediates the influx of Ca^{2+} and does not form intercellular dye coupling between HeLa Unx1 transfected cells. Unx1 channel function was further evidenced by its ability to mediate ionic currents when expressed in *Xenopus* oocytes. Downregulation of Unx1 mRNA with morpholine contains *Trypanosoma cruzi* invasion. Phylogenetic analysis revealed the presence of Unx1 homologs in other protozoan parasites, suggesting a conserved function for these channel parasites in other protists. Our data demonstrate that Unx1 forms large-pore membrane channels, which may serve as a diffusional pathway for ions and small molecules that are likely to be metabolic substrates or waste products, and signaling autocrine and paracrine molecules that could be involved in cell invasion. As morpholinos-induced downregulation of Unx1 reduces the infectivity of trypomastigotes, the Unx1 channels might be an attractive target for developing trypanocide drugs.

large membrane pore | gating | diffusional transport | unicellular organism | Trypanosoma cruzi

Large-pore channels exist in various tissues and organs in multicellular organisms, in gap-junctional and nongap-junctional forms, and serve essential physiological and pathophysiological functions (1). Large-pore channels are structures formed by several protein families including connexin (Cx), pannexin (Panx), innexin (Inx), calcium homeostasis modulator, and leucine-rich repeat-containing 8 proteins (2). Despite little sequence homology or no evolutionary linkage, large-pore channel members have similar transmembrane topologies with four similarly arranged transmembrane helices with different regulatory mechanisms (1, 3, 4). For example, it has been described that the activity of Panx1-formed channels increases in response to high $[K^+]_o$, oxygen–glucose deprivation, hypertonic conditions, or exposure to caffeine (4–7). Also, the removal of the C terminus and activation of α1D-adrenoreceptors also induces ATP release and cationic dye uptake without a major change in single-channel conductance and rectifying properties in Panx1 hemichannels (8). Recently, it has been described that mechanical stretch–dependent activation of Panx1 in physiological conditions involves the activation of Piezo1 channels and submembrane increase in Ca^{2+} signal, followed by phosphorylation of the S394 by CaMKII (9). However, Panx and Cx channels are structurally distinct (1). These forms of cell–cell communication in invertebrate organisms are mediated by protein subunits called Inx (10, 11). The activity of Inx-formed hemichannels increases in response to mechanical stress, elevated $[K^+]_o$, membrane depolarization, or increased cytoplasmic Ca^{2+} concentrations (10, 12, 13). By contrast, the Inx-formed hemichannel function is attenuated by arachidonic acid (14), lipopolysaccharide (15), and cytoplasmic acidification (12, 13). Also, pharmacological studies indicate that Inx-formed channels are inhibited by carbenoxolone (CBX) in a concentration-dependent way (12, 15) and Brilliant blue G (12–14). In silico studies have recently unraveled the existence of equivalent functional large-pore channel homologs in unicellular organisms of the family *Trypanosomatidea*; however, their gating mechanisms are yet to be demonstrated in cells (11).

The *Trypanosomatidae* are a group of unicellular, flagellated parasites, including many important pathogens of humans and animals (11). Interestingly, *Trypanosoma cruzi*

Significance

It is shown that *Trypanosoma cruzi* encodes an evolutionarily conserved membrane channel formed by a protein called unnexin1 (Unx1). Unx1 is a protein subunit of membrane channels permeable to small molecules and ions including Ca^{2+}, providing evidence that unicellular organisms, from the very early stage of evolution, have acquired the molecular mechanism for diffusion of ions and small molecules across the cell membrane, which could play a critical role in metabolism, and/or autocrine and paracrine cell signaling. Downregulation of *T. cruzi* trypomastigote Unx1 drastically reduces parasite cell invasion, suggesting a role for Unx1 in *T. cruzi* invasion and virulence, opening the way for the development of modulators with potential chemotherapeutic value for the control of human *Trypanosoma* infections.

(*T. cruzi*), a causal agent of Chagas disease (16–18) has been shown to inhibit Cx gap junction–mediated intercellular communication in cardiac myocytes, brown adipocytes, astrocytes, and leptomeningeal cells (19–22). As described in a recent study, *T. cruzi* infection increases Panx1 hemichannel activity in Hela-Panx1 cells and probenecid-sensitive dye uptake in neonatal rat cardiac myocytes (21). Blockers of Panx1 hemichannels, such as the mimetic peptide [10]Panx1 or probenecid, inhibit parasite-induced $[Ca^{2+}]_i$ transients and parasite invasion of host cells (21). Although the existence of large-pore homologs in unicellular organisms has been proposed (11), they are yet to be demonstrated in cells. In 2005, Gugssa and colleagues examined the cell–cell interactions between *Trypanosoma musculi* and murine splenic adherent fibroblast cells (23). These authors provided indirect evidence of heterocellular gap junction formation by observing fluorescence in parasites incubated with murine fibroblasts previously loaded with Lucifer yellow (23). Recently, we proposed that Unx proteins are members of the large-pore channel superfamily and are expressed in unicellular organisms (11). Unx proteins are closer to Inxs, sharing a secondary structure and the Inx-conserved motif YYQWV (11). In the present study, we demonstrate that one Unx protein is a subunit of the parasite large-pore channel that is required for *T. cruzi* invasion.

Results

Unnexin (Unx) Is a Transmembrane Protein That Forms Large-Pore Channels in the Membrane. In a previous in silico study, we identified five Unxs in *T. cruzi* (11). To assess subcellular localization, we cloned Unx1 (unnexin1) (XP_803915) fused to an enhanced green fluorescent protein (EGFP) in the carboxy-termini (CT) domain and performed confocal microscopy of HeLa cells transfected with Unx1-EGFP. Subsequently, the plasma membrane was labeled with a primary anti-Na$^+$/K$^+$ ATPase antibody and a secondary antibody fused to Alexa568 (Fig. 1*A*). Na$^+$/K$^+$ ATPase was mainly detected in the cell membrane, whereas Unx1-EGFP was detected in the cell membrane and intracellular compartments (Fig. 1*A*). Colocalization was observed in the membrane areas of the Na$^+$/K$^+$ ATPase and Unx1-EGFP cells (Fig. 1*A*) and the Pearson index for colocalization was $r = 0.5$ (Fig. 1 *A*, *Bottom*), suggesting that Unx1 is a membrane protein (Fig. 1*A*). Additionally, we cotransfected HEK-293T cells with a plasmid containing EGFP-Unx1 and plasmids encoding a monomeric red fluorescent protein (mRFP) fused to pmRFP-ß-1-4 galactosyltransferase (pmRFP-Golgi) or chromogranin A (pmRFP-CgA) to assess whether Unx1 was trafficked to the plasma membrane. Confocal immunofluorescence showed that EGFP-Unx1 partially colocalized with pmRFP-Golgi, indicating that Unx1 is associated with membrane structures in heterologously expressed cells and follows the classical pathway of membrane proteins (Fig. 1*B*). Moreover, Unx1 did not colocalize with CgA (Fig. 1*C*), suggesting that Unx1 is not a secreted protein. Using the web-based tool Protter (24), we predicted that Unx1 contains four transmembrane domains with intracellular C and N termini (Fig. 1*F*). To confirm this prediction, we used an anti-EGFP antibody to recognize Unx1 C terminus and designed antibodies to recognize the N terminus and the putative intracellular loop (Fig. 1*F*). Immunoreactive sites were evaluated by indirect immunofluorescence in nonpermabilized and permeabilized HeLa cells. Notably, the antibodies yielded a positive signal only in permeabilized cells, indicating that both the N and C termini as well as the protein domain that connects transmembranes 2 and 3 are located intracellularly (Fig. 1*D*).
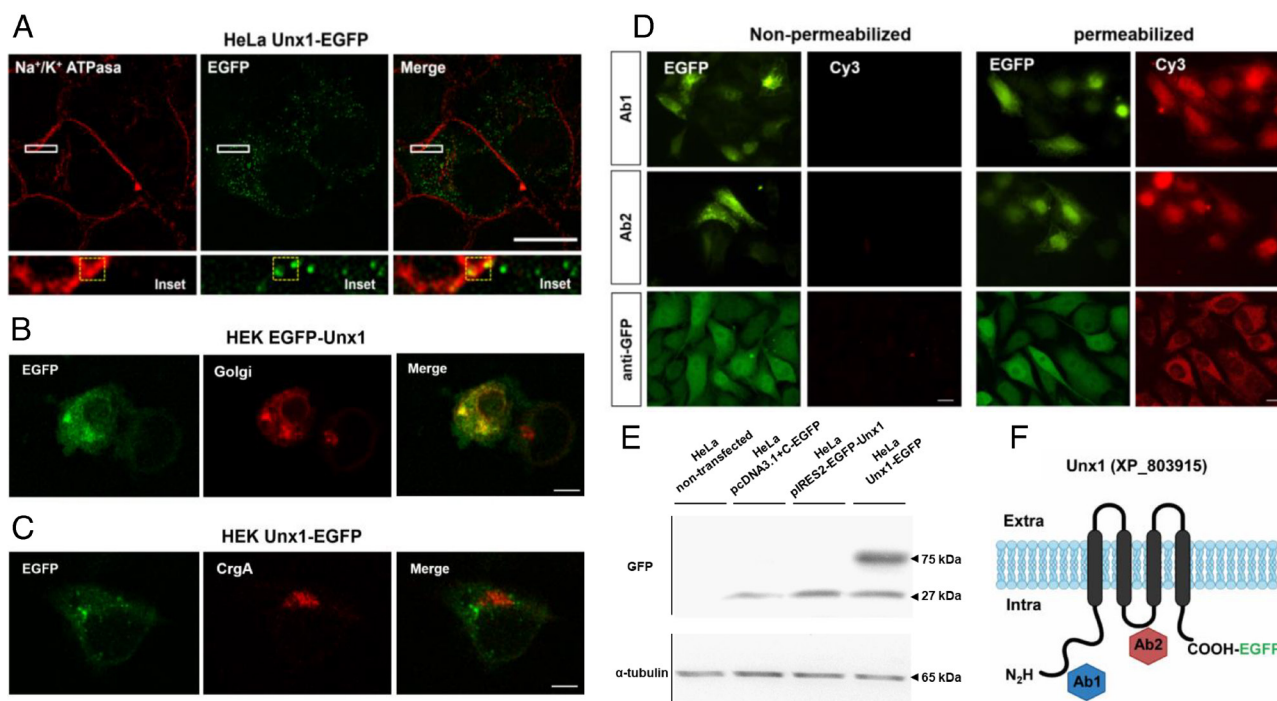

Fig. 1. Unx1 is a membrane protein with a conserved topology among members of the large-pore channel family. (*A*) Superresolution analysis of Unx1-EGFP localization in HeLa transfectants. Anti-α1 Na$^+$/K$^+$ATPase antibody was used as membrane marker, whose immunofluorescence was colocalized with that of EGFP fused to Unx1. The yellow box in the merge (bottom 6.5× amplification of rectangle denoted in the above panel) corresponds to the area of evaluation of the Pearson correlation index. (*B* and *C*) HEK293T cells were cotransfected with EGFP-Unx1 and pmRFP fused to ß-1-4 galactosyltransferase (Golgi) (*B*) or to CgA (*C*) to assess whether the Unx protein traffics to the plasma membrane. (*D*) Confocal immunofluorescence of HeLa cells transfected with the pcDNA3.1-Unx1-EGFP vector using rabbit anti-Unx1 antibodies (Abs#1 or #2) or anti-EGFP. Cy3 anti-rabbit signals were only detected in permeabilized cells treated with 0.01% Triton X-100, confirming the presence of intracellular epitopes. (Scale bar, 20 μm.) (*E*) Western blot analysis of total proteins evaluated with anti-EGFP antibody (1:1,000) from Cx45$^{-/-}$ HeLa cells 24 h after transfection with different Unx1 constructs, as shown in the figure. Anti- a-tubulin was used as the loading control. (*F*) Schematic representation of the proposed topology for Unx1 in the cell membrane, highlighting the N and C termini in intracellular space.

In the western blot analysis of total cell homogenates, we detected a single band of approximately 27 kDa corresponding to EGFP protein in samples of Cx45$^{-/-}$ HeLa cells transfected with pcDNA3.1+C-EGFP or pIRES-EGFP-Unx1 vector, whereas a ~75-kDa band was detected in cells transfected with pcDNA-Unx1-EGFP vector (HeLa Unx1-EGFP), which corresponds to the sum of the molecular weights of Unx1 (~55 kDa) plus EGFP (27 kDa) (Fig. 1E).

Unx Expression Increases Membrane Permeability to Small Molecules and Is Enhanced by Low Concentrations of Extracellular Divalent Cations or an Alkaline pH. Changes in extracellular divalent cation concentration, mechanical stretch, or pH can regulate the activity of some large-pore channel members, such as Cx43 (connexin 43) or Panx1 channels (25–27). To examine the relationship between $[Ca^{2+}]_o$, $[Mg^{2+}]_o$, and Unx1 channel activity, Unx1-expressing HeLa cells were bathed in a solution lacking Ca^{2+} and Mg^{2+} divalent cation free solution (DCFS), and DAPI uptake was measured over time (Fig. 2A). Exposure to DCFS increased DAPI uptake in Unx1-EGFP cells (0.40 ± 0.07 A.U./min vs. 0.06 ± 0.02 A.U./min), a response that was drastically reduced by 200 µM La^{3+} (0.17 ± 0.06 A.U./min), a blocker of Cx hemichannels (28), or 200 µM CBX (0.20 ± 0.02 A.U./min), a blocker of Panx1 and Cx hemichannels (29–31), and was absent in cells not transfected (0.05 ± 0.01 A.U./min vs. 0.02 ± 0.01 A.U./min) or transfected with the empty vector (HeLa pcDNA3.1+C-EGFP) (0.08 ± 0.02 A.U./min vs. 0.05 ± 0.01 A.U./min) (Fig. 2 A and B), suggesting that Unx1 forms membrane channels permeable to small molecules and is blocked by agents known to inhibit other large-pore channels. To further understand the gating mechanism that controls the activity of Unx1 channels, we tested the effects of mechanical stretching and an alkaline pH (8.5). Exposure to pH 8.5 increased the DAPI uptake rate (0.12 ± 0.01 A.U./min vs. 0.04 ± 0.001A.U./min) (*SI Appendix*, Fig. S1A). However, the mechanical stretching did not significantly affect this effect (0.09 ± 0.04 A.U./min vs. 0.06 ± 0.04 A.U./min) (*SI Appendix*, Fig. S1B). Notably, cells transfected with Panx1 showed an increase in DAPI uptake rate, which was completely inhibited by ^{10}Panx1 (0.40 ± 0.20 A.U./min vs. 0.04 ± 0.02 A.U./min) (*SI Appendix*, Fig. S1B). Neither of the stimuli used modified DAPI uptake rate in untransfected cells or cells transfected with the corresponding empty vector, and La^{3+} did not significantly affect DAPI uptake in these cells (See *SI Appendix*, Fig. S1 *A and B*, respectively). To assess possible interference from the EGFP tag, we transfected HeLa cells with the bicistronic vector pIRES2-EGFP-Unx1 and exposed them to DCFS. Under these conditions, the DAPI uptake rate increased significantly only in HeLa cells transfected with the bicistronic vector (0.20 ± 0.05 A.U./min vs. 0.07 ± 0.06 A.U./min), and was absent in cells untransfected or transfected with the empty vector. The dye uptake observed in cells transfected with the bicistronic vector was reduced to basal values by La^{3+} (uptake rate of 0.05 ± 0.01 A.U./min) (*SI Appendix*, Fig. S2A).

Next, we tested whether Unx1 channels are permeable to Ca^{2+}. The intracellular concentration of free Ca^{2+} in trypomastigotes has been shown to be between 10 and 20 nM (32, 33), and the extracellular concentration of this ion in host organisms is between 1.5 and 2.0 mM, generating a strong driving force toward the intracellular compartment. To explore if Unx1 channels are permeable to Ca^{2+}, HeLa cells transfected with Unx1 (Unx1-EGFP cells) were exposed to pH 8.5 in Mg^{2+}-free solution containing either 3 mM or 5 mM Ca^{2+} to further increase the gradient of this ion across the cell membrane. Beyond a slight tendency to increase, this condition did not produce significant changes in the Fura 2-AM signal in HeLa Unx1-EGFP cells. The increase of Fura 2-AM emission in pH 8.5 in Mg^{2+}-free solution containing 5 mM
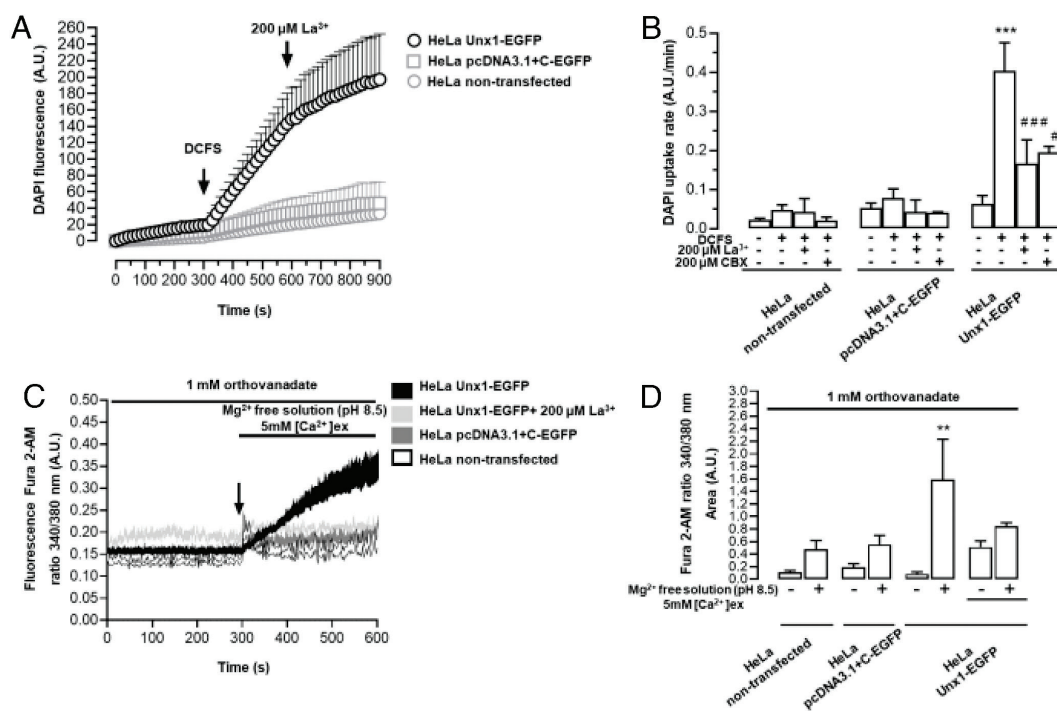

Fig. 2. The Unx1 channel activity is increased by low extracellular concentration of divalent cations, and Ca^{2+} permeates the channels. (*A*) Time-course of DAPI uptake was evaluated in parental and Cx45 KO HeLa cells transfected with Unx1. The absence of extracellular Ca^{2+} and Mg^{2+} (DCFS) increased DAPI uptake, which was blocked by 200 µM lanthanum (La^{3+}) or CBX. (*B*) Ca^{2+} signal (ratio of fluorescence emission at 340 and 380 nm) was evaluated in HeLa Unx1-EGFP cells loaded with Fura-2 and exposed to an extracellular solution without Mg^{2+}, pH 8.5, and containing 1 mM orthovanadate (*C* and *D*). Data are presented as mean ± SEM; ***$P < 0.001$ vs. basal. ##$P < 0.01$, ###$P < 0.001$ vs. DCFS (n = 3 to 8).

Ca^{2+} was 1.59 ± 0.64 A.U. in HeLa Unx1-EGFP vs. 0.48 ± 0.14 A.U. HeLa nontransfected (*SI Appendix*, Fig. S2B). To avoid the possible involvement of plasma membrane Ca^{2+} (PMCA) pumps in handling the increase in intracellular Ca^{2+} induced by the above conditions, we applied an Mg^{2+}-free extracellular solution in the presence of 1 mM sodium orthovanadate, as described previously (25). After stimulation, Fura 2-AM fluorescence intensity increased steadily in Unx1-transfected cells compared to basal conditions (Fig. 2 *C* and *D*). This increase was prevented by treatment with 200 μM La^{3+} (Fig. 2 *C* and *D*). This increase in Fura 2-AM fluorescence was not observed in cells transfected with the empty vector or in nontransfected HeLa cells (Fig. 2 *C* and *D*), suggesting that Unx1 channels could mediate the influx of Ca^{2+}, increasing the intracellular concentration of this divalent ion.

Unx Expression Induces Voltage-Dependent Plasma Membrane Conductance. It has been previously shown that membrane currents increase at positive voltages in channels formed by Cxs or Panxs (13, 34). To directly test the ability of Unx1 to facilitate ion flux across the plasma membrane, *Xenopus laevis* oocytes were used to express Unx1 cRNA (Fig. 3). We measured the macroscopic ionic currents in oocytes injected with cRNAs 3 to 4 d before recording. Macroscopic currents were induced in oocytes expressing Unx1 protein by holding the membrane voltage at –40 mV and then applying voltage pulses of 5 s from –40 to +100 mV in 10 mV increments. Depolarizing pulses induced large outward currents in Unx1-expressing oocytes that were blocked by lanthanum ions (Fig. 3*A*). At 100 mV pulse, the outward current exceeds 3 μA (mean ± SEM) when recorded with the cut-open oocyte technique and was reduced when exposed to 250 μM La^{3+}. In the same

batch of oocytes, the outward currents observed after injection with a 10-fold dilution of Unx1 cRNA were less prominent and equally sensitive to La^{3+}, indicating that the outward current was determined by the amount of Unx1 coding mRNA. Since Cx38 is endogenously expressed by *Xenopus* oocytes and could form hemichannels (35), we also recorded outward currents in oocytes coinjected with antisense Cx38 RNA and Unx1 cRNA and recorded ionic currents with an intact intracellular milieu using the traditional 2-electrode voltage-clamp technique (Fig. 3*D*). In Fig. 3*E*, we show that voltage-dependent current induced in oocytes injected with Unx1 cRNA, and antisense Cx38 RNA were reduced by rising extracellular Ca^{2+}. Thus, the expression of Unx1 induces voltage-dependent plasma membrane conductance that is sensitive to extracellular Ca^{2+} and La^{3+}.

HeLa Cells Transfected with Unx1 Do Not Form Gap Junction Channels. Some Cxs, Inxs, and recently Panx1 are known to form gap junction channels (4, 36). We explored whether Unx1 forms gap junction intercellular communications in HeLa Unx1-EGFP cells (*SI Appendix*, Fig. S3). Evaluating the intracellular passage of ethidium bromide (EtBr) or sulforhodamine 101 (SR101), after 5 min of EtBr microinjection into one cell of a cluster of Unx1-expressing cells, the dye did not spread to neighboring cells (*SI Appendix*, Fig. S3A). The incidence coupling index was 1.23 ± 0.09 (A.U.) vs. 1.13 ± 0.07 (A.U.) or 1.56 ± 0.09 (A.U.) for cells transfected with the empty vector or nontransfected cells, respectively (*SI Appendix*, Fig. S3A). HeLa Cx43-EGFP used as a positive control showed a coupling index of 11.5 ± 1.72 (A.U.) (*SI Appendix*, Fig. S3A). Similar results were observed with SR101 dye (a negatively charged dye), no passage of dye to neighboring
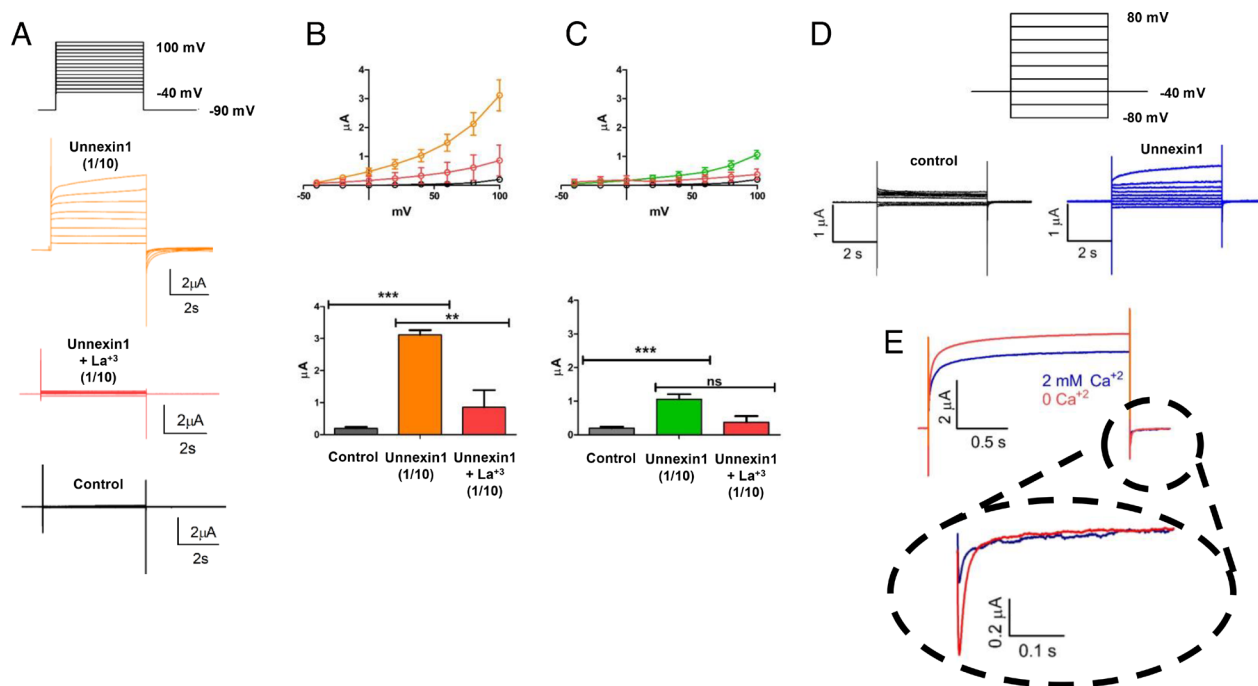

Fig. 3. Unx1-mediated macroscopic currents are sensitive to voltage. Unx1-expressing oocytes were recorded using the cut-open oocyte technique (*A–C*) and two-electrode voltage clamp (*D* and *E*). (*A*) Representative traces of currents obtained with the voltage-pulse protocol depicted on the top from a batch of oocytes with negligible endogenous currents (control), injected with a 1/10 dilution of Unx1 mRNA before (orange) and after adding La^{3+} to a final concentration of 250 μM. (*B*) Current vs. voltage (IV) plots and maximal current (*Bottom*) obtained from the same batch of oocytes shown in *A* injected with 1/10 dilution of Unx1 mRNA in the absence (orange, n=13) and presence of 250 μM La^{3+} (red; n = 5; **$P < 0.05$ and ***$P < 0.001$). (*C*) As *B* from oocytes injected with a 1/100 dilution of Unx1 mRNA in the absence (green, n = 6) and presence of 250 μM La^{3+} (red; n = 3; ***$P < 0.002$). For comparison, we included measurements from uninjected oocytes (gray; n = 16) of the same batch. (*D* and *E*) Electrophysiological recordings of Unx1-expressing oocytes obtained by the two-electrode oocyte technique. Representative traces of currents were obtained with the holding protocol –40 mV from –80 mV at intervals of 20 mV to 80 mV from a batch of oocytes coinjected with Unx1 1/10 dilution of mRNA and anti-Cx38 antisense. (*E*) Reduction of Unx1 induced current by extracellular Ca^{2+}. Representative traces in the absence (orange) and presence of 2 mM Ca^{2+} in the bath solution. In the presence of extracellular Ca^{2+} both, the outward and tail inward current evoked by a pulse to +80 mV and repolarization to –40 mV, respectively, were reduced by approximately 30% and 60%.

cells at 5 min postinjection was observed in HeLa Unx1-EGFP cells (incidence index 1.17 ± 0.09 A.U.). This result was similar to those cells transfected with the empty vector (incidence index 1.10 ± 0.06 A.U.) and nontransfected cells (incidence index 1.10 ± 0.10 A.U.) but contrary to the HeLa Cx43-EGFP cell line (incidence index 8.37 ± 0.94 A.U.) (*SI Appendix*, Fig. S3B). These findings suggest that Unx1 does not form gap junction channels in the transfected HeLa cells.

Unx Participle in *T. cruzi* Invasion. To study the participation of Unx1 in *T. cruzi* invasion, Vero cells were used to evaluate the infectivity of trypomastigotes pretreated with antisense complementary oligonucleotide morpholinos against Unx1. In cells infected with trypomastigotes previously transfected with antisense complementary oligonucleotide morpholinos directed against Unx1 (antisense), the number of amastigotes, ovoid form of 1 to 5 µm long by 1 to 2 µm wide, was significantly reduced to 54 ± 12 parasites/500 cells compared to 148 ± 25 parasites/500 cells under controlled conditions, arrows in the inset, trypomastigotes transfected with the control morpholinos and nontransfected trypomastigotes (*SI Appendix*, Fig. S4)]. Also, La^{3+}, which blocked the DAPI uptake mediated by Unx1 channels (Fig. 2) also reduced the number of infected Vero cells to values similar to those recorded in Vero cells infected with trypomastigotes pretreated with antisense morpholinos (*SI Appendix*, Fig. S4).

Discussion

In this study, we showed that *T. cruzi* Unx1 encodes an evolutionarily conserved membrane channel that exhibits structural and biophysical properties similar to those of human large-pore channels. Our data indicate that Unx1 is a protein subunit of membrane channels permeable to small molecules and ions, such as Ca^{2+}, providing evidence that unicellular organisms, from the very early stage of evolution, have acquired the molecular mechanism for diffusion pathway related to substrates and metabolites, as well as relevant signaling molecules and ions driven by gradient concentrations, which play a critical role in metabolism, and/or autocrine and paracrine cell signaling.

The expression of Unx1 protein was demonstrated by immunofluorescence detection of immunoreactive epitopes used to generate antibodies and by western blot analysis of bands with electrophoretic mobility close to that of Unx1-EGFP. The colocalization of Unx1 with Na^+/K^+ ATPase in domains of the cell membrane and lack of colocalization with CgA revealed that Unx1 can be found in the cell membrane, which is supported by functional studies reported herein, and is not a secreted protein. The observed intracellular Unx1 reactivity corresponded to Unx1 trafficking either to or from the cell membrane, which was supported by the colocalization of EGFP-Unx1 with pmRFP-Golgi, indicating that Unx1 is associated with the membrane structures of organelles that follow the classical traffic pathway of membrane proteins. Accordingly, Unx1 besides being at the cell membrane as demonstrated here, may also be located in specific intracellular organelles of *T. cruzi*. Proteomic studies have identified the Unx1 sequence in *T. cruzi* contractile vacuole membrane proteins (37), which are involved in osmoregulation in *T. cruzi* (38). This function could be relevant because the highest mRNA levels of Unx1 have been predicted in the epimastigote stage (39), a stage that could be exposed to osmolarities of 600 to 1,000 mOsm in the vector intestine (40), suggesting a possible role for the channel in the osmoregulation mechanisms of the parasite. Interestingly, the participation of channels formed by Inx11 in osmoregulation processes in *Schmidtea mediterranea* has been described (41).

Although the role of Unxs in osmoregulation was not evaluated in this study, we previously showed that high osmolarity (600 mOsm) increases DAPI uptake in epimastigotes of *T. cruzi* (11), so it is important to consider the possible role of Unx1 channels in this process in future studies.

Our in silico and experimental studies using the web-based tool Protter and antibodies directed to different domains of the wild-type or EGFP-fused protein revealed that in the cell membrane, Unx1 presents C- and N-terminal domains facing the intracellular space, with four transmembrane domains leaving two extracellular and one intracellular loop that connects transmembrane regions. Because Cxs, Panx, and Inxs have similar membrane topologies and do not share relevant sequence homology with Unxs. All the homologs identified in the Trypanosomatidae parasites only exhibited the Inx motif YYQWV (42), which was found primarily on presumptive transmembrane domain 3 (11). This suggests that spatial conformation might play a relevant role in preserving similar functions despite the lack of sequence homology. Further studies will be required to determine whether the spatial conformation is related to the physicochemical features of the channels including the electrostatic profile across the channel and permeability properties.

The inflow of DAPI, a small and charged molecule, upon application of different chemical stimuli (low concentration of extracellular divalent cations and alkaline pH), revealed that the activity of Unx1 channels can be regulated by variations in the external microenvironment. Moreover, voltage enhanced the membrane current elicited by oocytes expressing Unx1, which may play a functional role when epimastigotes are exposed to high concentrations of osmolytes, thereby affecting resting membrane potential.

We observed the development of voltage-dependent ionic currents in oocytes injected with Unx1 cRNA in a concentration-dependent manner (RNA dilution), in the absence of extracellular Ca^{2+}. The voltage dependency of Unx1 channel seems to be unipolar (Fig. 3); it exhibits a monotonic progression as the membrane depolarization increases across both the negative and positive voltage ranges and does not inactivate at more positive potentials, which is different from the one reported for many Cxs, including Cx38 that is bipolar because of the appearance of inactivation at more positive potentials (43). This current was reduced by 2 mM Ca^{2+}, similarly as previously reported for the hemichannels formed by Cxs, Unx1 activity is regulated by the extracellular Ca^{2+} concentration and, to some extent, extracellular Mg^{2+} (44), as observed in dye uptake experiments. In Cx46 channels, extracellular Ca^{2+} binds to two negatively charged residues (glutamic acid 48 and aspartic acid 51), disrupting the electrostatic network and favoring a closed state (45). However, an increase in extracellular Mg^{2+} changes the voltage dependence of activation to more positive potentials (44).

The increase in DAPI uptake induced by extracellular solution at pH 8.5 is similar to the increase in activity of Panx1 and Cx43 hemichannels (25). This effect was even observed in the presence of physiological concentrations of extracellular Ca^{2+}, suggesting that this mechanism is insensitive to extracellular Ca^{2+} (close to 2 mM Ca^{2+}). Is it possible that an alkaline pH releases the induced inhibition of Unx1 channels induced by Ca^{2+}? A possible explanation may be the pH-induced displacement of Ca^{2+} bound to channel domains that reduce activity. An alkaline pH would favor the formation of calcium hydroxide, $Ca(OH)_2$, reducing the amount of soluble Ca^{2+} and therefore reducing its inhibitory action on Unx1 channels. In contrast to this possibility, we observed an increase in the intracellular Ca^{2+} signal in cells loaded with Fura-2 exposed to pH 8.5, indicating that enough Ca^{2+} was present to promote its own passage through the Unx1 channels.

Thus, it is conceivable that pH 8.5, induces a conformational change in Unx1 channels, making inaccessible the Ca^{2+}-binding domains of the channel and thus, favoring its cellular influx.

López and coworkers proposed a mechanism by which mechanical stimulation increases the activity of Panx1 hemichannels (46). This mechanism consists of a submembrane increase in intracellular Ca^{2+}, mediated through Piezo1 mechanosensitive channels that contribute to the activation of the Ca^{2+}/calmodulin-dependent kinase II (CaMK II) pathway with consequent phosphorylation of a Serine394 residue in the C-terminal domain of Panx1 (46). Interestingly, although the presence of homologs of piezo channels and CaMK proteins in *T. cruzi* has been reported (47, 48), the bioinformatic analysis in our previous work showed that Unx1 has only a putative phosphorylation site by Protein kinase A (PKA) and Protein kinase C (PKC), but not by CaMK II (11). This finding is consistent with the results obtained in the present study, in which mechanical stimulation did not influence the Unx1 channel activity.

Most Cxs and Inxs can form gap junction channels that connect neighboring cells (36, 49). In the present study, no passage of small fluorescent dyes (positively or negatively charged) was observed in HeLa Unx1-EGFP cells, suggesting that Unx1 channels did not form gap junction channels. Cysteine residues have been proposed to reside in the extracellular loops of Cx32, and are critical for gap junction channel formation via intramolecular disulfide bonds with the extracellular loop from a neighboring cell (50, 51). This would depend on the redox state of these cysteines because the addition of a reducing agent decreases the currents mediated by Cx32-based gap junction channels (50). Cxs and Inxs contain three conserved cysteine residues in their extracellular loops (52). However, the putative Unx1 topology does not reveal the presence of extracellular cysteine residues (11). This observation could explain why Unx1 transfectants did not exhibit the intercellular passage of dyes. Alternatively, the conditions that favor the formation of Unx1 gap junction channels should be determined in future studies.

Large-pore channels participate in Ca^{2+} signaling in several tissues, and some have even been described as permeable to Ca^{2+} (25, 53). Ca^{2+} signaling pathways are essential for *T. cruzi* invasion (33, 54, 55). For instance, an increase in cytosolic-free Ca^{2+} in trypomastigotes occurs during the early stages of the invasion (54, 55). In addition, the loading of the parasites with Ca^{2+} chelators, such as bis-(o-aminophenoxy)-ethane-N, N, N′, N′-tetraacetic acid or ethylene glycol tetraacetic acid (EGTA), resulted in a decreased ability to invade the myoblasts (33, 54). The cytosolic-free Ca^{2+} present in trypomastigotes is between 20 and 30 nM (33), and the extracellular concentration of this ion in host organisms is between 1.5 and 2.0 mM, generating a strong electrochemical potential toward the intracellular compartment. Therefore, we believe that an Unx channel could be a possible gateway for extracellular Ca^{2+} entry in *T. cruzi*.

SI Appendix, Fig. S5 shows the results of a phylogenetic analysis of 30 putative protein sequences homologous to *T. cruzi* Unx 1 from different genera of parasitic *trypanosomatids* that present high sequence similarity. These homologous sequences can be divided into two main branches, one incorporating *Phytomonas*, *Strignomonas*, and *Agnomonas*, and the other *Trypanosoma*, *Leptomonas*, and *Leishmania* genus, suggesting that Unx1 is broadly distributed between protists of the *Trypanosomatidae* family characterized by causing human infectious diseases such as Chagas' disease, African sleeping sickness, and leishmaniasis, affecting approximately 20 million people worldwide (56). Some species also affect farm animals and plants (genus *Phytomonas*), causing enormous economic loss. Further studies are required to determine whether Unx1 is a common mechanism of infection among these taxa. Finally, it has been proposed that Inx proteins are primordial gap-junction molecules, while Cxs have evolved more recently in deuterostomes (57).

However, because unicellular organisms appear on earth approximately 3.5 million years ago and multicellular organisms only 600 million years ago, it is possible that Unx1 represents an early ancestor of Inxs. Consistently, all Unx proteins possess the canonical motif of the Inx family, the pentapeptide YYQWV (11).

Materials and Methods

Ethics Statement. All experiments were performed in strict accordance with the manual's recommendations of biosecurity standards and the associated risks of Comisión Nacional de Investigación Científica y Tecnológica (CONICYT) Chile (2018), and were approved by the Institutional Ethics Committee of Universidad de Antofagasta-Chile (N°109-2018).

Reagents. CBX disodium salt (#C4790), lanthanum chloride (La^{3+}), and SR101 were obtained from Sigma-Aldrich (St. Louis, MO). FURA 2-AM, Dulbecco's modified Eagle medium (DMEM), and geneticin (G418) were obtained from Thermo Fisher Scientific (Waltham, MA, USA). 4′,6-diamidino-2-phenylindole (DAPI) was obtained from Tocris Biosciences (Bristol, UK). EtBr and Fluoromont-G were obtained from Thermo Fisher Scientific (Waltham, MA, USA). Collagenase was obtained from the Worthington Biochemical Corporation (Lakewood, NJ, USA). Ethyl 3-amino-benzoate methanesulfonic acid salt.

Antibodies. The rabbit anti-Unx1 polyclonal antibodies were obtained from Fucited (Santiago, Chile). Goat anti-rabbit IgG antibody conjugated to AlexaFluo568 (A-11036) was obtained from Thermo Fisher Scientific (Waltham, MA, USA). Goat anti-rabbit IgG antibody conjugated with Cy3 was obtained from Jackson ImmunoResearch (West Grove, PA, USA). Goat anti-rabbit IgG antibody conjugated to horseradish peroxidase was obtained from Santa Cruz Biotechnology (Dallas, TX, USA). Rabbit anti-human Na^+/K^+ ATPase monoclonal antibody (ab76020) and mouse anti-green fluorescent protein monoclonal antibody (ab1218) were obtained from Abcam (Cambridge, MA, USA).

Cell Culture and Transfection. HeLa and human embryonic kidney (HEK-293T) cells were cultured in DMEM supplemented with fetal bovine serum (10%) and penicillin–streptomycin (50 U/mL) and maintained at 37 °C under 5% CO_2. HeLa Panx1-EGFP and HeLa Cx43-EGFP cells were cultured with geneticin (1 mg/mL) to maintain stable transfection. HeLa parental cells were obtained from the American Type Culture Collection, HeLa Panx1-EGFP was provided by Dr. Felixas Bukaukas (Department of Neuroscience, Albert Einstein College of Medicine, Bronx, NY, USA), and HeLa Cx43-EGFP was provided by Dr. Klaus Willecke (Bonn University, Bonn, Germany). Cells were plated on glass coverslips (25-mm diameter) in 35-mm dishes at approximately 2×10^5 cells per dish. Vero cells were grown in RPMI supplemented with 10% fetal bovine serum and maintained at 37 °C under 5% CO_2.

Plasmids and Transfection. Unx1 fused to EGFP in its N-terminal domain was inserted into the mammalian pCDNA3.1 + c-EGFP expression vector using the BamHI and NotI restriction enzymes. In addition, Unx1 was subcloned in the pIRES2EGFP vector, between NheI and EcoRI restriction sites. Plasmids (4 µg) were resuspended in serum-free DMEM (400 µL) and 10 µL of TurboFect reagent was added. The transfection mixture was incubated for 30 min at room temperature and then it was drip-added onto HeLa cells previously seeded on glass coverslips (25-mm diameter) at 70% confluence (46). The plasmids used were pβ1, 4GALT1:mRFP-W, expressing β-1,4-galactosyl transferase:mRFP to label the Golgi apparatus and pmRFP:ChrgA-W, expressing mRFP:Chromogranin-A to label dense core vesicles.

Dye Uptake and Time-Lapse fluorescence imaging. Cells were incubated in Krebs solution (in mM: 118 NaCl; 4.7 KCl; 1.2 KH_2PO_4; 1.2 $MgSO_4$; 4.2 $NaHCO_3$; 2 $CaCl_2$; 10 glucose and 10 HEPES) at pH 7.4, which containing 5 µM DAPI. Fluorescence intensity at regions of interest (ROI) was obtained in real-time (every 30 s) using a Nikon inverted fluorescence microscope (Melville, NY, USA), and the images were analyzed with Image J software. The background value was subtracted for each ROI value.

Electrophysiology. Female frogs were anesthetized with 0.5% ethyl 3-amino-benzoate methanesulfonic acid salt, and the oocytes were removed, defolliculated by 1- to 2-h treatment with 3 mg/mL collagenase at room temperature, washed, and kept at 18 °C in oocyte Ringer's pH 7.4 solution (in mM: 96 mM NaCl, 2 mM

KCl, 1.8 mM CaCl$_2$, 1 mM MgCl$_2$, 5 mM HEPES). Each oocyte was injected with 50 nL of 1 mg/mL cRNA by using a microinjection system (Nanoliter 2000; World Precision Instruments). Ionic currents were recorded 3 to 4 d after cRNA injection. Electrophysiological recordings of Unx1-expressing oocytes were performed using either the cut-open technique with a CA-1B amplifier (Dagan Corp., Minneapolis, MN, USA), as previously described (58) or 2-electrode voltage-clamp. The external solution contained 82 mM NaCl, 5 mM 4-(2-hydroxyethyl)-1-piperazineethanesulfonic acid (HEPES), 1 mM MgCl$_2$, and 2.5 mM KCl. The internal solution for the cut oocytes contained: 120 mM KCl, 10 mM HEPES, 10 mM EGTA, pH 7.0. Currents measurements and I/V relationships were accomplished using the cut-open oocyte technique with the holding protocol −90 mV from −40 mV in intervals of 20 mV to 100 mV and the two-electrode oocyte technique with the holding protocol –40 mV from −80 mV in intervals of 20 mV to 80 mV. Data acquisition and analysis were performed using an in-house script running in MATLAB and digitized using NI-USB-6341 (National Instruments, Austin, TX, USA). The currents were filtered at 2 kHz and digitized at 10 kHz.

Estimation of Intracellular Free Ca^{2+} Signals. We estimated the free [Ca^{2+}]$_i$ with Fura 2-AM (Molecular Probes, Eugene, OR) as described previously (46). In brief, cells were incubated for 30 min at 37 °C in Krebs solution pH 7.4, (in mM: 118 NaCl; 4.7 KCl; 1.2 KH$_2$PO$_4$; 1.2 MgSO$_4$; 4.2 NaHCO$_3$; 2 CaCl$_2$; 10 glucose, and 10 HEPES) containing 5 μM of the membrane-permeant AM ester form of Fura 2-AM dissolved in dimethyl sulfoxide (DMSO). The cells were then washed three times with PBS (phosphate-buffered saline), and fluorescence images (ratio 340/380 nm) were captured every 1 s using a Nikon inverted microscope equipped with a 40× objective and NIS software (Melville, NY, USA).

Immunofluorescence and Confocal Microscopy. Cells grown on coverslips were fixed at room temperature with 4% paraformaldehyde for 10 min and washed three times with PBS. The cells were incubated for 4 h at room temperature with an anti-Unx1 polyclonal antibody (1:200) diluted in 0.1% PBS–Triton X-100 solution with 0.121 mM NH$_4$Cl and 1% BSA (bovine serum albumin). Subsequently, the cells were washed three times with 0.1% PBS–Triton X-100 and then incubated for 1 h at room temperature with rabbit anti-mouse IgG conjugated with Cy3 (1:500). After several washes, coverslips were mounted in Fluoromount-G with DAPI, and fluorescence images were captured using a Nikon D-Eclipse C1 confocal microscope equipped with NIS software (Melville, NY, USA). Stacks of consecutive confocal images were taken at 2-μm intervals. For membrane localization, cells were seeded on 10-mm diameter glass coverslips, transfected using the protocol described above, fixed with 70% methanol for 30 min at 4 °C, washed four times, and permeabilized with 0.5% Triton X-100 for 30 min. They were then blocked with 1% BSA, incubated for 12 h with rabbit anti-Na$^+$/K$^+$ ATPase mAb (1:300), washed four times, incubated for 1 h with goat anti-rabbit IgG + Alexa Fluor 568 (1:300), washed four times, and mounted with Fluoromount G + DAPI. Superresolution images were obtained in the Z-plane every 1.5 μm using a superresolution laser microscope (ELYRA-SIM Zeiss) with a Plan-Apochromat 63×/1.4 Oil DIC M27 objective lens. The Pearson correlation index was calculated to assess the colocalization between EGFP and Alexa 568 using the ImageJ software.

Parasite Culturing. *T. cruzi* Y strain was used in all experiments (59). To obtain tissue culture–derived trypomastigotes (TCTs), Vero cells were infected with trypomastigotes in a parasite-to-cell ratio of 5:1 for 3 h. The cultures were then washed and incubated in RPMI 1640 medium supplemented with 2% fetal bovine serum (21). After 5 d, culture supernatants highly enriched in TCTs were collected by centrifugation and used in further experiments.

Cell Invasion Assay. Vero cells were seeded at a density of 5 × 10^4 cells/well in 4-well Lab-Tek Chamber Slides (Thermo Fisher Scientific, Roskilde, Denmark). The TCT invasion assay was conducted as previously reported (21), using a parasite: cell ratio of 5:1. After incubation for 3 h, Vero cells were washed 3× with PBS, fixed with paraformaldehyde, and stained with propidium iodide. The number of amastigotes within 500 cells was determined using a BX51 fluorescence microscope (Olympus Corporation, Tokyo, Japan).

Generation of Antisense Complementary Oligonucleotide Morpholinos. Third-generation antisense complementary oligonucleotide morpholinos were used as described previously (52). For Unx1, the antisense primer was 5′-ATAATGCCTTCTTCTCCCATCATCA-3′, and the antisense mispair control was 5′-ATAT TCCCTTGTTCTGCGATCATCA-3′. Parasites (1 × 10^5) were incubated for 18 h with 10

μM morpholino and 6 μM Endo-Porter according to the manufacturer's protocol. Trypomastigotes treated with sense or antisense morpholine were used in the in vitro invasion assay.

Phylogenetic Tree of Putative Unx Sequences. For phylogenetic analysis 30 protein sequences were used that had between 35% and 100% identity or similarity (amino acid substitutions with conserved physicochemical characteristics, for example, one positive charge for another positive charge, etc.) with respect to the Unx1 query protein sequence from *T. cruzi* (XP_803915.1) obtained after BLASTP search against the National Center for Biotechnology genomic protein databases. Several of these sequences are hypothetical, that is to say, they are derived or predicted by analysis of the genome of the different organisms, and they would be orthologous to Unx1 characterized in this study.

The sequences used were: *Trypanosoma brucei gambiense* (XP_011778195), *Trypanosoma brucei brucei* (XP_823075), *Trypanosoma brucei equiperdum* (RHW69224), *Trypanosoma congolense* (CCC93953), *Trypanosoma vivax* (KAH8620505), *Trypanosoma grayi* (XP_009309094), *Trypanosoma theileri* (XP_028879643), *Trypanosoma melophagium* (KAH9578085), *T. cruzi* (XP_803915), *Trypanosoma rangeli* (AGN32920), *Trypanosoma conorhini* (XP_029228294), *Leishmania major* (XP_001687221), *Leishmania infantum* (XP_001469356), *Leishmania mexicana* (XP_003874991), *Leishmania tarentolae* (GET93734), *Leishmania brazilensis* (XP_001569275), *Leishmania panamensis* (XP_010703575), *Leishmania guyanensis* (CCM19889), *Leishmania martiniquensis* (KAG5464478), *Leishmania enrietti* (KAG5465960), *Leishmania namibia* (KAG5489063), *Leishmania orientalis* (KAG5465220), *Leishmania ghana* (KAG5489798), *Leptomonas seymouri* (KPI8706), *Leptomonas pyrrhocoris* (XP_015660242), *Bodo saltans* (CUG94230), *Phytomonas sp EM1* (CCW63246), *Phytomonas sp Hart1* (CCW70047), *Strigomonas culicis* (EPY31113), and *Angomonas deanei* (CAD2213252). To generate a phylogenetic tree for the 30 putative Unx1 orthologs, multiple sequence alignments we performed using the MUSCLE method (60). The tree was constructed based on the sequence alignment of the amino acid sequence of putative Unx1 orthologs considering 346 amino acid positions of the conserved domains by the Neighbor-Joining method using the Jones–Taylor–Thornton substitution matrix and with the rate variations among the sites corresponding to a gamma value = 1.1. Bootstrap statistics were used at the branching points after 500 iterations or in replicates. Bootstrap values of less than 30 were not considered. Both alignments and phylogenetic trees were generated using MEGA version 11 (61).

Statistical Analysis. The results are expressed as mean ± SEM, and significant statistical differences between groups were determined using a two-way ANOVA with Tukey's post hoc test to perform multiple comparisons. Prism 8 software (GraphPad Inc., California, USA) was used for the graphs and statistical analyses. Differences were considered significant at *P* values lower than 0.05.

Data, Materials, and Software Availability. All study data are included in the article and/or *SI Appendix*.

Author affiliations: [a]Laboratory of Gap Junction Proteins and Parasitic Diseases (GaPaL), Instituto Antofagasta, Universidad de Antofagasta, Antofagasta 1240000, Chile; [b]Laboratorio de Microorganismos Extremófilos, Instituto Antofagasta, Universidad de Antofagasta, Antofagasta 1240000, Chile; [c]Departamento de Tecnología Médica, Unidad de Parasitología Molecular, Facultad Ciencias de la Salud, Universidad de Antofagasta, Antofagasta 1240000, Chile; [d]Instituto de Neurociencias, Centro Interdisciplinario de Neurociencias de Valparaíso, Facultad de Ciencias, Universidad de Valparaíso, Valparaíso 2381850, Chile; and [e]Departamento Biomédico, Facultad de Ciencias de la Salud, Universidad de Antofagasta, Antofagasta 1240000, Chile

1. E. C. Beyer, V. M. Berthoud, Gap junction gene and protein families: Connexins, innexins, and pannexins. *Biochim. Biophys. Acta Biomembr.* **1860**, 5–8 (2018).
2. J. Syrjanen, K. Michalski, T. Kawate, H. Furukawa, On the molecular nature of large-pore channels. *J. Mol. Biol.* **433**, 166994 (2021), 10.1016/j.jmb.2021.166994.
3. S. Locovei, L. Bao, G. Dahl, Pannexin 1 in erythrocytes: Function without a gap. *Proc. Natl. Acad. Sci. U.S.A.* **103**, 7655–7659 (2006).
4. N. Palacios-Prado *et al.*, Endogenous pannexin1 channels form functional intercellular cell-cell channels with characteristic voltage-dependent properties. *Proc. Natl. Acad. Sci. U.S.A.* **119**, e2202104119 (2022).
5. L. Bao, S. Locovei, G. Dahl, Pannexin membrane channels are mechanosensitive conduits for ATP. *FEBS Lett.* **572**, 65–68 (2004).
6. M. C. Kienitz, K. Bender, R. Dermietzel, L. Pott, G. Zoidl, Pannexin 1 constitutes the large conductance cation channel of cardiac myocytes. *J. Biol. Chem.* **286**, 290–298 (2011).
7. R. J. Thompson, N. Zhou, B. A. MacVicar, Ischemia opens neuronal gap junction hemichannels. *Science* **312**, 924–927 (2006).
8. Y. H. Chiu *et al.*, A quantized mechanism for activation of pannexin channels. *Nat. Commun.* **8**, 14324 (2017).
9. X. López *et al.*, Stretch-induced activation of pannexin 1 channels can be prevented by PKA-dependent phosphorylation. *Int. J. Mol. Sci.* **21**, 9180 (2020).
10. J. Güiza, I. Barria, J. C. Sáez, J. L. Vega, Innexins: Expression, regulation, and functions. *Front. Physiol.* **9**, 1414 (2018).
11. J. Güiza *et al.*, Unnexins: Homologs of innexin proteins in Trypanosomatidae parasites. *J. Cell Physiol.* **237**, 1547–1560 (2022).
12. L. Bao *et al.*, Innexins form two types of channels. *FEBS Lett.* **581**, 5703–5708 (2007).
13. G. Dahl, K. J. Muller, Innexin and pannexin channels and their signaling. *FEBS Lett.* **588**, 1396–1402 (2014).
14. S. E. Samuels, J. B. Lipitz, J. Wang, G. Dahl, K. J. Muller, Arachidonic acid closes innexin/pannexin channels and thereby inhibits microglia cell movement to a nerve injury. *Dev. Neurobiol.* **73**, 621–631 (2013).
15. K. Luo, M. W. Turnbull, Characterization of nonjunctional hemichannels in caterpillar cells. *J. Insect Sci.* **11**, 6 (2011).
16. C. Bern, S. P. Montgomery, An estimate of the burden of Chagas disease in the United States. *Clin. Infect Dis.* **49**, e52–e54 (2009).
17. C. Chao, J. L. Leone, C. A. Vigliano, Chagas disease: Historic perspective. *Biochim. Biophys. Acta Mol. Basis Dis.* **1866**, 165689 (2020).
18. J. A. Perez-Molina, I. Molina, Chagas disease. *Lancet* **391**, 82–94 (2018).
19. A. C. Campos de Carvalho *et al.*, Gap junction disappearance in astrocytes and leptomeningeal cells as a consequence of protozoan infection. *Brain Res.* **790**, 304–314 (1998).
20. A. C. de Carvalho *et al.*, Gap junction distribution is altered between cardiac myocytes infected with *Trypanosoma cruzi*. *Circ. Res.* **70**, 733–742 (1992).
21. I. Barria *et al.*, *Trypanosoma cruzi* infection induces pannexin-1 channel opening in cardiac myocytes. *Am. J. Trop. Med. Hyg.* **98**, 105–112 (2018).
22. S. Burke *et al.*, Adipocytes in both brown and white adipose tissue of adult mice are functionally connected via gap junctions: Implications for Chagas disease. *Microbes Infect.* **16**, 893–901 (2014).
23. A. Gugssa *et al.*, Co-culture of Trypanosoma musculi with spleen-derived adherent fibroblasts: Possible transfer of small molecules via connexons. *J. Submicrosc. Cytol. Pathol.* **37**, 223–229 (2005).
24. U. Omasits, C. H. Ahrens, S. Muller, B. Wollscheid, Protter: Interactive protein feature visualization and integration with experimental proteomic data. *Bioinformatics* **30**, 884–886 (2014).
25. K. A. Schalper *et al.*, Connexin 43 hemichannels mediate the Ca²⁺ influx induced by extracellular alkalinization. *Am. J. Physiol. Cell Physiol.* **299**, C1504–C1515 (2010).
26. P. A. Harcha *et al.*, Pannexin-1 channels are essential for mast cell degranulation triggered during type I hypersensitivity reactions. *Front. Immunol.* **10**, 2703 (2019).
27. V. K. Verselis, M. Srinivas, Divalent cations regulate connexin hemichannels by modulating intrinsic voltage-dependent gating. *J. Gen. Physiol.* **132**, 315–327 (2008).
28. J. A. Orellana *et al.*, Cation permeation through connexin 43 hemichannels is cooperative, competitive and saturable with parameters depending on the permeant species. *Biochem. Biophys. Res. Commun.* **409**, 603–609 (2011).
29. K. Michalski, T. Kawate, Carbenoxolone inhibits pannexin1 channels through interactions in the first extracellular loop. *J. Gen. Physiol.* **147**, 165–174 (2016).
30. K. Michalski *et al.*, The Cryo-EM structure of pannexin 1 reveals unique motifs for ion selection and inhibition. *elife* **9**, e54670 (2020).
31. E. A. Turovsky, E. G. Varlamova, M. V. Turovskaya, Activation of Cx43 hemichannels induces the generation of Ca²⁺ oscillations in white adipocytes and stimulates lipolysis. *Int. J. Mol. Sci.* **22**, 8095 (2021).
32. R. Docampo, S. N. Moreno, A. E. Vercesi, Effect of thapsigargin on calcium homeostasis in *Trypanosoma cruzi* trypomastigotes and epimastigotes. *Mol. Biochem. Parasitol.* **59**, 305–313 (1993).
33. S. N. Moreno, J. Silva, A. E. Vercesi, R. Docampo, Cytosolic-free calcium elevation in *Trypanosoma cruzi* is required for cell invasion. *J. Exp. Med.* **180**, 1535–1540 (1994).
34. J. E. Contreras, J. C. Sáez, F. F. Bukauskas, M. V. Bennett, Gating and regulation of connexin 43 (Cx43) hemichannels. *Proc. Natl. Acad. Sci. U.S.A.* **100**, 11388–11393 (2003).
35. L. Ebihara, Xenopus connexin38 forms hemi-gap-junctional channels in the nonjunctional plasma membrane of Xenopus oocytes. *Biophys. J.* **71**, 742–748 (1996).
36. B. C. Bennett *et al.*, An electrostatic mechanism for Ca²⁺-mediated regulation of gap junction channels. *Nat. Commun.* **7**, 8770 (2016).
37. P. N. Ulrich *et al.*, Identification of contractile vacuole proteins in *Trypanosoma cruzi*. *PLoS One* **6**, e18013 (2011).
38. P. Rohloff, R. Docampo, A contractile vacuole complex is involved in osmoregulation in *Trypanosoma cruzi*. *Exp. Parasitol.* **118**, 17–24 (2008).
39. Y. Li *et al.*, Transcriptome remodeling in *Trypanosoma cruzi* and human cells during intracellular infection. *PLoS Pathog.* **12**, e1005511 (2016).
40. S. Bonansea *et al.*, Stress response to high osmolarity in *Trypanosoma cruzi* epimastigotes. *Arch. Biochem. Biophys.* **527**, 6–15 (2012).
41. N. J. Oviedo, M. Levin, smedinx-11 is a planarian stem cell gap junction gene required for regeneration and homeostasis. *Development* **134**, 3121–3131 (2007).
42. P. Phelan, Innexins: Members of an evolutionarily conserved family of gap-junction proteins. *Biochim. Biophys. Acta.* **1711**, 225–245 (2005).
43. I. Fasciani *et al.*, Regulation of connexin hemichannel activity by membrane potential and the extracellular calcium in health and disease. *Neuropharmacology* **75**, 479–490 (2013).
44. L. Ebihara, X. Liu, J. D. Pal, Effect of external magnesium and calcium on human connexin46 hemichannels. *Biophys. J.* **84**, 277–286 (2003).
45. W. López *et al.*, Mechanism of gating by calcium in connexin hemichannels. *Proc. Natl. Acad. Sci. U.S.A.* **113**, E7986–E7995 (2016).
46. X. López *et al.*, A physiologic rise in cytoplasmic calcium ion signal increases pannexin1 channel activity via a C-terminus phosphorylation by CaMKII. *Proc. Natl. Acad. Sci. U.S.A.* **118**, e2108967118 (2021).
47. S. Ogueta, G. M. Intosh, M. T. Tellez-Inon, Regulation of Ca²⁺/calmodulin-dependent protein kinase from *Trypanosoma cruzi*. *Mol. Biochem. Parasitol.* **78**, 171–183 (1996).
48. D. L. Prole, C. W. Taylor, Identification and analysis of putative homologues of mechanosensitive channels in pathogenic protozoa. *PLoS One* **8**, e66068 (2013).
49. A. Oshima, T. Matsuzawa, K. Nishikawa, Y. Fujiyoshi, Oligomeric structure and functional characterization of *Caenorhabditis elegans* Innexin-6 gap junction protein. *J. Biol. Chem.* **288**, 10513–10521 (2013).
50. G. Dahl, E. Levine, C. Rabadan-Diehl, R. Werner, Cell/cell channel formation involves disulfide exchange. *Eur. J. Biochem.* **197**, 141–144 (1991).
51. S. Rahman, W. H. Evans, Topography of connexin32 in rat liver gap junctions. Evidence for an intramolecular disulfide linkage connecting the two extracellular peptide loops. *J. Cell Sci.* **100**, 567–578 (1991).
52. A. Sánchez, C. Castro, D. L. Flores, E. Gutierrez, P. Baldi, Gap junction channels of innexins and connexins: Relations and computational perspectives. *Int. J. Mol. Sci.* **20**, 2476 (2019).
53. A. J. Moreno-Ortega *et al.*, CALHM1 and its polymorphism P86L differentially control Ca²⁺ homeostasis, mitogen-activated protein kinase signaling, and cell vulnerability upon exposure to amyloid beta. *Aging Cell* **14**, 1094–1102 (2015).
54. I. Tardieux, M. H. Nathanson, N. W. Andrews, Role in host cell invasion of *Trypanosoma cruzi*-induced cytosolic-free Ca²⁺ transients. *J. Exp. Med.* **179**, 1017–1022 (1994).
55. N. Yoshida, Molecular basis of mammalian cell invasion by *Trypanosoma cruzi*. *An. Acad. Bras Cienc.* **78**, 87–111 (2006).
56. P. J. Hotez, Human parasitology and parasitic diseases: Heading towards 2050. *Adv. Parasitol.* **100**, 29–38 (2018).
57. H. Alexopoulos *et al.*, Evolution of gap junctions: The missing link? *Curr. Biol.* **14**, R879–R880 (2004).
58. A. Neely, J. García-Olivares, S. Voswinkel, H. Horstkott, P. Hidalgo, Folding of active calcium channel beta(1b)-subunit by size-exclusion chromatography and its role on channel function. *J. Biol. Chem.* **279**, 21689–21694 (2004).
59. J. San Francisco *et al.*, *Trypanosoma cruzi* pathogenicity involves virulence factor expression and upregulation of bioenergetic and biosynthetic pathways. *Virulence* **13**, 1827–1848 (2022).
60. R. C. Edgar, MUSCLE: Multiple sequence alignment with high accuracy and high throughput. *Nucleic Acids Res.* **32**, 1792–1797 (2004).
61. S. Kumar, G. Stecher, M. Li, C. Knyaz, K. Tamura, MEGA X: Molecular evolutionary genetics analysis across computing platforms. *Mol. Biol. Evol.* **35**, 1547–1549 (2018).